ACS APPLIED MATERIALS & INTERFACES

Research Article

www.acsami.org

Engineering Graphene Conductivity for Flexible and High-Frequency Applications

Alexander J. Samuels[†] and J. David Carey*[,‡]

[†]Advanced Technology Institute and [‡]Department of Electrical and Electronic Engineering, University of Surrey, Guildford, GU2 7XH, United Kingdom

ABSTRACT: Advances in lightweight, flexible, and conformal electronic devices depend on materials that exhibit high electrical conductivity coupled with high mechanical strength. Defect-free graphene is one such material that satisfies both these requirements and which offers a range of attractive and tunable electrical, optoelectronic, and plasmonic characteristics for devices that operate at microwave, terahertz, infrared, or optical frequencies. Essential to the future success of such devices is therefore the ability to control the frequency-dependent conductivity of graphene. Looking to accelerate the development of high-frequency applications of graphene, here we demonstrate how readily accessible and processable organic and organometallic molecules can efficiently dope graphene to carrier densities in excess of 10^{13} cm^{-2} with conductivities at gigahertz frequencies in excess of 60 mS. In using the molecule 3,6-difluoro-2,5,7,7,8,8-hexacyanoquinodimethane (F2-HCNQ), a high charge transfer (CT) of 0.5 electrons per adsorbed molecule is calculated, resulting in p-type doping of graphene. n-Type doping is achieved using cobaltocene and the sulfur-containing molecule tetrathiafulvalene (TTF) with a CT of 0.41 and 0.24 electrons donated per adsorbed molecule, respectively. Efficient CT is associated with the interaction between the π electrons present in the molecule and in graphene. Calculation of the high-frequency conductivity shows dispersion-less behavior of the real component of the conductivity over a wide range of gigahertz frequencies. Potential high-frequency applications in graphene antennas and communications that can exploit these properties and the broader impacts of using molecular doping to modify functional materials that possess a low-energy Dirac cone are also discussed.

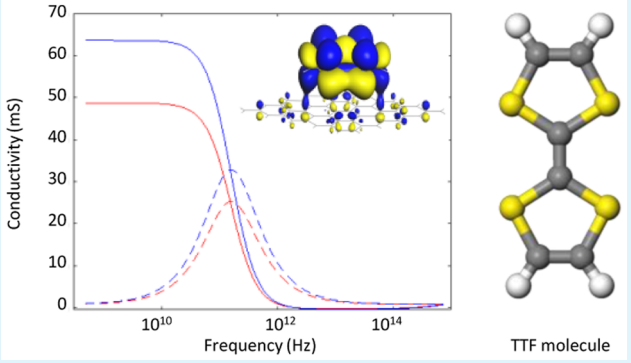

KEYWORDS: *graphene engineering, molecular doping, TTF, DDQ, F2-HCNQ, Dirac cone materials, high-frequency conductivity, graphene antennas*

1. INTRODUCTION

Two-dimensional layered materials and devices are one of the most active areas of current nanomaterials research[1] and encompass such diverse materials as graphene,[2] hexagonal boron nitride, black phosphorus (phosphorene),[3] silicene,[4] the transition-metal dichalcogenides,[5] and a wide range 2D layered oxide materials.[6] As a family of functional materials they offer considerable potential to exploit a number of attractive electronic and optoelectronic properties by taking advantage of their inherent 2D structure as semiconductors or conductors, either as a single layer or as few layers with a stacking-order- and number-dependent band gap or as part of a vertical (sandwich) or in-plane lateral heterostructure. Single-layer graphene is the best known of the 2D layered van der Waals materials, and the continued research excitement surrounding graphene is a reflection of the ongoing successful advances in large-area, high-quality material production using chemical vapor deposition (CVD) and related techniques, of the ability to successfully transfer graphene to technologically important substrates with minimal damage and residual contamination, and of sustained improvements in material and device processing, as well as successful surface chemical functionalization strategies. The distinctive low-energy linear band dispersion of single-layer graphene leads to quasiparticles that mimic the characteristics of massless Dirac fermions, which propagate with a Fermi velocity (v_F) that is about $^1/_{300}$ of the speed of light.[2] These properties have led to high room-temperature carrier mobilities,[2] a distinctive quantum Hall and Landau level spacing behavior,[7] and a largely wavelength-independent visible optical absorption. Graphene has already demonstrated some of these properties, serving variously as a calibration for universal constants,[8] as a transparent contact in solar cells,[9] in high-frequency electronic devices with high power gain cutoff frequencies up to 100 GHz,[10] in mid-IR and terahertz plasmonics,[11] and as tunable nanoantennas that do not suffer from enhanced grain boundary scattering often found in small-scale metal-based antennas.[12] More generally, a timeline of graphene applications, in the form of a roadmap,

Received: June 10, 2015
Accepted: September 21, 2015
Published: September 21, 2015

DOI: 10.1021/acsami.5b05140
ACS Appl. Mater. Interfaces 2015, 7, 22246−22255

has been established that identifies the key stages of introduction of a range of electronic and photonic devices.[13] Future envisaged devices include highly flexible displays,[14] devices based on saturable absorption leading to ultrafast lasers, optical frequency converters, and low-noise high-speed (50 GBits/s) wafer-scale produced photodetectors,[15] as well as conformal antennas and terahertz devices.[16] In the latter devices, the frequency-dependent conductivity is controlled by intraband and interband absorption transitions between non-Pauli (state) blocked states.

Having the ability to control the carrier concentration in graphene and operate devices away from the Dirac point (E_D) is a key requirement for many of the envisaged applications. Around E_D, where the occupied (π) and unoccupied (π^*) states meet, the net carrier concentration in unbiased devices is controlled by substrate-induced local puddles of charge density. p- or n-Type doping, which shifts the Fermi level (E_F) away from E_D, can be accomplished by electrostatic gating, through polarization on ferroelectric periodically poled lithium niobate substrates,[17] by charge transfer from the inclusion of substitutional atoms,[18] or through decoration by adatoms[19] or molecules.[20] Adsorption of atoms or molecules with a high binding energy onto graphene's surface is therefore an attractive route to permanently shift E_F away from E_D, and the use of local patterning techniques, such as electron beam writing or dip pen nanolithography, allows for the further modification of the electrical, plasmonic, and optical properties.[21] Examples of the use of small (environmental) molecule adsorption to dope graphene include exposure to NH_3 vapor (for n-type doping) or NO_2 (for p-type), though the efficiency of the charge transfer (defined as the change in carrier density per concentration of molecules adsorbed) can be low, as discussed below.[22,23] Large values of charge transfer per adsorbed molecule are required to enhance the electrical conductivity for applications such as transparent conductors, as a metal-free catalyst in the oxygen reduction reaction in fuel cells, for applications where an underlying electrostatic gate is not possible on a flexible substrate, or where a gate electrode is not required. Examples of molecular or polymer materials employed for efficient charge transfer include the use of self-assembled monolayers of fluoropolymer FTS (fluoroalkyltrichlorosilane, $C_8H_4F_{13}SiCl_3$) to p-dope graphene[24] or the use of extended doping layers of the piezoelectric polymer poly(vinylidene fluoride-*co*-trifluoroethylene) [P(VDF-TrFE)]. Graphene/P(VDF-TrFE)/graphene sandwich structures have already successfully been employed to act as a flexible transparent acoustic actuator and nanogenerator in which the polymer layer acts as a strong n-type dopant and can reduce the graphene sheet resistance to below 190 Ω/sq;[25] more generally, P(VDF-TrFE) can act as a nonvolatile ferroelectric substrate combining good optical transparency, mechanical strength, and flexibility.[26]

Optimization and control of the amount of charge transfer from an adsorbed species is thus an important practical consideration for many potential graphene applications where the Fermi level needs to be shifted away from the zero density of states (DOS) Dirac point. Measurements of the electrical properties arising from the physisorption of small molecules on graphene show that the charge transfer per molecule can be low with, for example, Romero et al. measuring a NH_3 doping efficiency (electrons donated per molecule adsorbed) of 0.068 ± 0.004.[23] Evidently, larger doping efficiencies are required for the applications discussed above, and here we show that this can be achieved through the controlled use of a small concentration (<2% molecule decoration) of π-electron-containing planar organic and organometallic molecules. n- and p-Type doping behavior can be obtained through determination of the energy level position of the molecule's frontier orbitals, namely, the highest occupied (HOMO) and lowest unoccupied molecular orbital (LUMO), relative to the Fermi energy of graphene, as explained in detail below. Organic and organometallic molecules can be adsorbed, via physisorption, onto graphene's surface with a high binding energy (0.4 − 1 eV), provided that there is a strong attractive interaction between the molecule's π electron cloud and the π electron cloud found in graphene. Novel doping approaches using molecular adsorption also have the key advantage of a mature processing technology, have potentially controllable decoration and patterning, and have been extensively employed in molecular electronic devices.[27] Local patterning and molecular engineering, which can be achieved using dip-pen lithography or e-beam lithography, allow for further selective spatial tunability. Our goal in this study is therefore (i) to investigate and quantify the charge transfer between π-electron-containing molecules physisorbed onto pristine single layer graphene, (ii) to identify efficient molecular dopant species, and (iii) to explore the effects on the high-frequency (GHz frequency band) conductivity that will accelerate the development of graphene devices. We have employed ab initio density functional theory (DFT) methods to quantify the charge transfer, to explore the resultant effects on the low-energy graphene band structure and the density of states surrounding the Dirac point, and to calculate the real and imaginary components of the frequency-dependent conductivity.

The simplest description of molecular doping of graphene is to consider the energy level position of the adsorbed molecule's frontier (HOMO and LUMO) orbitals, relative to the graphene Fermi level. When the energy of the HOMO level is above E_F, direct n-type doping from the occupied states of the molecule to the unoccupied states of graphene occurs; direct p-type doping occurs when the energy of the LUMO level is below E_F. This is the description of direct or resonant charge transfer involving the molecule's frontier orbitals; an indirect (off-resonance) charge transfer mechanism can result, arising from hybridization of the molecule's orbitals with graphene's orbitals. If this mixing is strong enough, this can result in n-type (p-type) doping, even if the energy of the HOMO (LUMO) level of the molecule is below (above) E_F; in this study we will distinguish between these two charge transfer mechanisms. We report in detail the behavior arising from the adsorption of two π-electron-containing metallocene molecules, cobaltocene and ferrocene, and three planar organic molecules, tetrathiafulvalene (TTF), 2,3-dichloro-5,6-dicyano-*p*-benzoquinone (DDQ), and 3,6-difluoro-2,5,7,7,8,8-hexacyanoquinodimethane (F2-HCNQ), all of which differ in their number of π electrons but all are readily commercially available with an established history of use in electronic devices.

2. COMPUTATIONAL DETAILS

The results presented here have been obtained using DMol[3] ab initio density functional theory code employing the Vosko−Wilk−Nusair functional within the local density approximation (LDA).[28] The calculations proceed by placing a single molecule above the graphene layer, and geometry optimization is performed until the force on each atom is less than 0.05 eV/Å in order to find the optimum adsorption separation and molecular configuration. The double-numeric with

DOI: 10.1021/acsami.5b05140
ACS Appl. Mater. Interfaces 2015, 7, 22246−22255

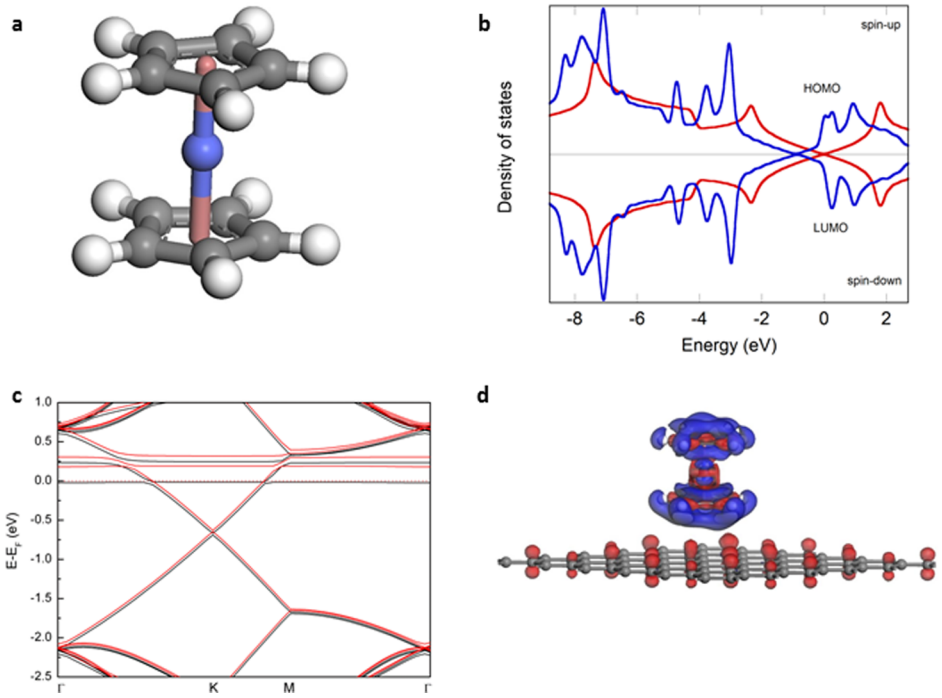

Figure 1. (a) Molecular structure of cobaltocene with the Co atom (colored blue) sandwiched between two cyclopentadienyl (Cp) anion rings. (b) Spin-polarized density of states of isolated graphene (red lines) and of $CoCp_2$ adsorbed on graphene (blue lines). The spin-polarized HOMO and LUMO levels are indicated. (c) The corresponding band structure of the graphene−$CoCp_2$ system with spin-up levels (red) and spin-down levels (black). (d) Isosurface with an isovalue of ±0.005 e/Å^3 of the change in the electron density when a cobaltocene molecule is adsorbed on a graphene surface; red areas (blue areas) represent increased (decreased) electron density, respectively.

polarization (DNP) basis set with an all-electron core treatment is employed for these calculations. A 6 × 6 single layer supercell consisting of 72 carbon atoms, corresponding to a molecular coverage of just 1.4% with a supercell area of 18.9×10^{-15} cm^2, is used for all the reported calculations. Reflecting the use of periodic boundary conditions, a separation of approximately 15 Å is used in order to avoid mutual interactions between the graphene layers. The potential energy, $E_{potential}$, is calculated at a range of separations in order to find the optimum intermolecular separation in the usual way

$$E_{potential} = E_{total} - E_{graphene} - E_{molecule} \quad (1)$$

where E_{total} is the total energy of the graphene−molecule system upon adsorption, $E_{graphene}$ is the energy of the graphene layer in the absence of the molecule, and $E_{molecule}$ is the energy of the molecule in the free state. The binding energy is defined as the magnitude of the minimum potential energy at the optimum intermolecular separation, where the intermolecular separation is taken from the center-of-mass of the molecule to the graphene layer. Some care must be exercised in the interpretation of the DFT results, as calculations using the LDA tend to overestimate molecular binding energy and underestimate the optimum intermolecular separation.[29] A key benchmark result is how well the calculations determine the molecule−graphene optimum separation. For a van der Waals system with physisorbed species, this separation should be about 3.2−3.3 Å. Charge transfers are calculated using the Hirshfeld charge partitioning method, and a negative (positive) charge transfer is defined here to imply n-type (p-type) doping of the graphene layer by the molecule. A 5 × 5 × 1 Monkhorst−Pack grid is used to sample the Brillouin zone in order to calculate the binding energy and charge transfer, and a 15 × 15 × 1 grid with a Gaussian smearing of 0.074 eV is used to calculate the DOS. The high symmetry points are labeled with the usual Brillouin zone labeling, not zone-folding notation.

3. RESULTS AND DISCUSSION

3.1. Metallocene Doping. Metallocene molecules consist of a divalent metal ion sandwiched between two cyclopentadienyl (Cp) anion rings (Figure 1a), where each Cp ring has six π electrons. The Cp rings have a low barrier to rotation around the central Cp-ring−metal−Cp-ring axis. Two of the most well-known metallocenes are cobaltocene ($CoCp_2$) and ferrocene ($FeCp_2$), and we find for both molecules the optimum separation between the closest cyclopentadienyl ring and graphene is 3.2 Å, a value typical of $\pi-\pi$ electron van der Waals stacked systems. The molecular binding energy on graphene is calculated to be 0.86 and 0.42 eV, respectively, accompanied by a charge transfer of −0.41 electron/molecule (n-type doping of graphene) and +0.003 holes/molecule (very weak p-type doping), respectively. Parts b and c of Figure 1 show the spin-polarized density of states and the band structure of cobaltocene (with 19 valence electrons in total) adsorbed on graphene, respectively. The partially occupied HOMO level is found at 0.7 eV above E_D, and has an electron occupancy of 0.51e, which is reduced from 1e found in the free molecule. The magnetic moment of the $CoCp_2$ molecule is also reduced from 1 μ_B to 0.48 μ_B, inducing a magnetic moment of 0.52 μ_B in the graphene layer due to charge donation from the spin-polarized HOMO orbital. Finally, it has been calculated that the Co−Cp bond length has shortened from 1.683 to 1.651 Å.

All of these results represent strong evidence of electron donation, which is also seen in the change in electron density on the graphene layer (Figure 1d). The increase in the electron density (red areas, Figure 1d), appears to be quite uniform across the carbon atoms in graphene, suggesting uniform layer doping. The depleted region of charge density surrounding the entire $CoCp_2$ molecule suggests that the charge is donated from all parts of the molecule, not just the closest Cp ring to the graphene layer, as the uppermost Cp ring lies almost 6.5 Å away from the layer. The spin-polarized impurity levels at the Fermi energy exhibit a dispersion-less behavior in the Brillouin zone

DOI: 10.1021/acsami.5b05140
ACS Appl. Mater. Interfaces 2015, 7, 22246−22255

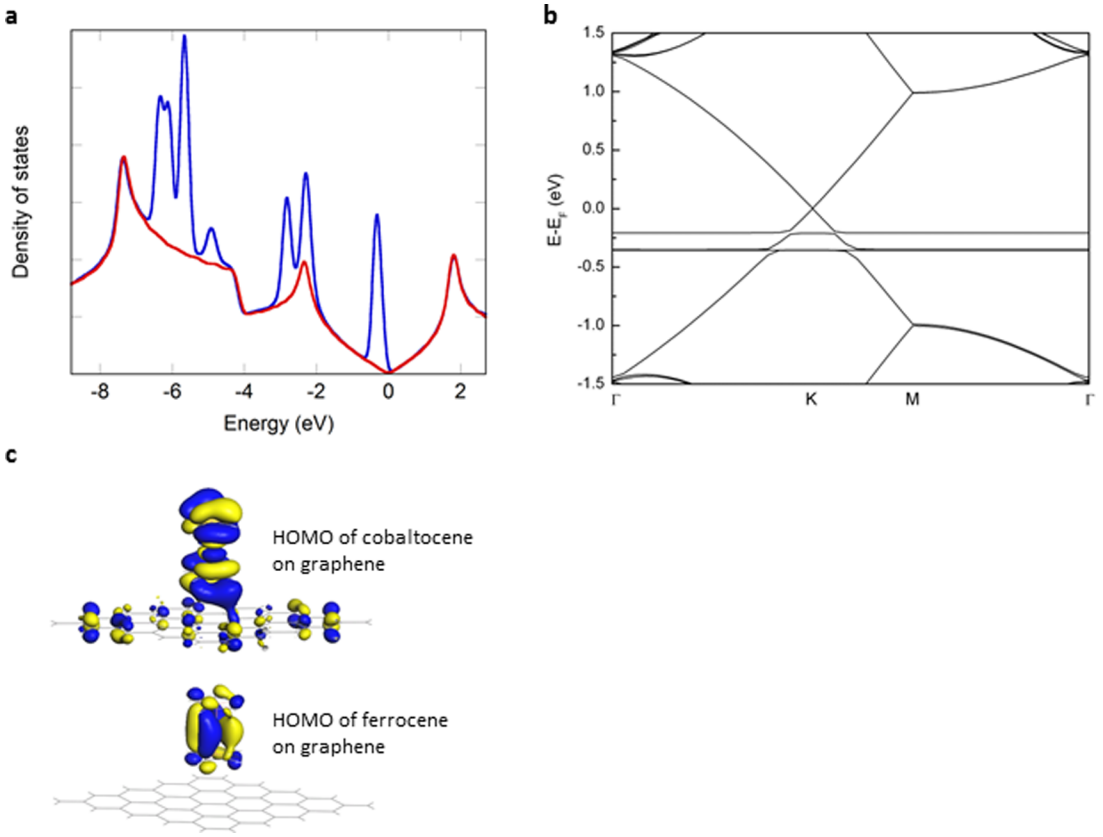

Figure 2. (a) Density of states of isolated graphene (red line) and of $FeCp_2$ adsorbed on graphene (blue line) and (b) the corresponding band structure of the graphene−$FeCp_2$ system. (c) The HOMO of $CoCp_2$ (upper figure) and $FeCp_2$ (lower figure) on graphene showing the effects on the graphene's π electron cloud upon adsorption.

(Figure 1c), apart from where the bands cross and the spin-split HOMO and LUMO are separated by about 0.3 eV; this compares to ∼0.5 eV energy separation calculated in the isolated molecule, suggesting a small change to the electron exchange−correlation energy upon adsorption.

In the case of $FeCp_2$ (18 valence electrons in total) adsorption on graphene, the Fe atom−graphene separation is about 4.9 Å, and the closest Cp ring to graphene separation is found to be 3.2 Å. Charge transfer analysis reveals negligible p-type doping, +0.003e/molecule, with a single broad impurity peak in the DOS just below the Dirac point (Figure 2a). The band structure (Figure 2b) shows that the broad impurity peak observed from the DOS calculations is actually composed of two closely spaced impurity energy levels, which span the Brillouin zone at energies just below the Fermi energy at E_F − 0.17 eV and E_F − 0.23 eV, respectively. No hybridization of graphene's bands is seen upon adsorption with either molecule, and in the case of $FeCp_2$, the HOMO orbital is found to be localized entirely on the molecule, whereas the HOMO of $CoCp_2$ adsorbed on graphene shows extensive changes to the π electron cloud (Figure 2c). Given that the Cp rings of $CoCp_2$ and $FeCp_2$ both contain the same number of π electrons, it might have been expected that the wave functions associated with the π electrons in the cyclopentadienyl ring and graphene would interact in a similar way. This evidently appears not to be the case, with direct charge transfer occurring for $CoCp_2$ adsorption, as the HOMO level is 0.7 eV above E_D (direct charge transfer), whereas doping is inhibited for $FeCp_2$ adsorption, as the HOMO level is 0.2 eV below the Dirac point. The LUMO of $FeCp_2$ on graphene is found to be several electronvolts above E_D and plays no role.

The presence of efficient charge transfer upon adsorption of $CoCp_2$ from a strongly bound species unaccompanied by significant disruption to the low-energy linear band structure has important implications for achieving a high carrier concentration without the introduction of low-energy (resonant) scattering centers,[30] where the perturbing potential would normally be sufficient to reduce carrier mobility and conductivity. We have also studied the adsorption of chromocene ($CrCp_2$) and manganocene ($MnCp_2$) on graphene, and these calculations reveal a moderate n-type doping behavior, 0.11e per $CrCp_2$ molecule and 0.04e per $MnCp_2$ molecule adsorbed, respectively. Analysis of their respective band structure and DOS reveals a behavior intermediate to that found upon adsorption of $CrCp_2$ and $FeCp_2$, respectively.

3.2. Organic Molecule Doping. Many planar hydrocarbon molecules can have many more π electrons than the metallocenes molecules, for example, TTF [$H_2C_2S_2C_2)_2$, Figure 3a] has a total of 14 π electrons. TTF is a sulfur-containing molecule consisting of two dithiolylidene rings with each ring contributing seven π electrons with each sp^2 C atom providing one π electron and an additional two π electrons arising from one of the lone pairs on each S atom; the second lone pair of electrons does not contribute to the π electron density. An ionization potential of 6.2 eV is calculated for TTF, and we find a binding energy of between 0.90 and 0.95 eV depending on the location of the center of the molecule relative to the graphene lattice. The highest binging energy of 0.95 eV is

DOI: 10.1021/acsami.5b05140
ACS Appl. Mater. Interfaces 2015, 7, 22246−22255

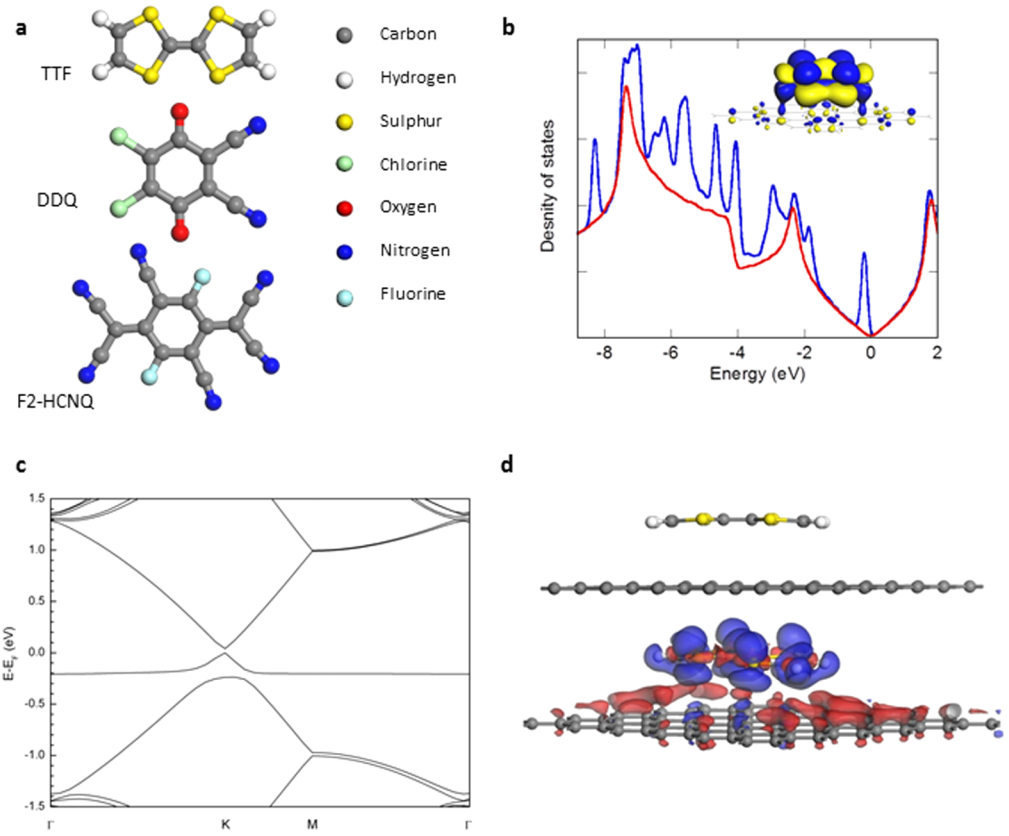

Figure 3. (a) Structure of the molecules TTF, DDQ, and F2-HCNQ with the atoms labeled, as per the color scheme. (b) Density of states of isolated graphene (red line) and of TTF adsorbed on graphene (blue line). Inset: HOMO of TTF on graphene. (c) Band structure of the graphene−TTF system. (d) Upper figure: geometry of the TTF molecule adsorbed on graphene shows that the outer hydrogen atoms are closer to the layer than the central carbon atoms. Lower figure: isosurface with an isovalue of ±0.002 e/Å^3 of the change in the electron density when a TTF molecule is adsorbed on a graphene surface; red areas (blue areas) represent increased (decreased) electron density.

found when the central carbon−carbon bond of TTF is over a graphene carbon−carbon bond. The high binding energy is a result of the strong π−π electron interaction with an optimum intermolecular separation of 3.3 Å. Adsorption of TTF on graphene is accompanied by n-type charge transfer of 0.21−0.24e/molecule, again depending on the TTF molecular registry on the graphene lattice. Figure 3b shows that the HOMO level of TTF on graphene lies 0.2 eV below the Dirac point; normally, the presence of a HOMO level below E_D would lead to a negligible direct doping efficiency, as in $FeCp_2$. However, the adsorption of TTF is accompanied by extensive delocalization of the HOMO (inset, Figure 3b) and significant band mixing with the appearance of a 0.3 eV band gap (Figure 3c). It is the efficient mixing between the TTF and graphene π orbitals that results in high charge transfer and to changes in the π electronic cloud (Figure 3d), despite the apparently unfavorable relative position of the frontier orbitals.

While TTF is found to be an n-type dopant, previous studies[31,32] of p-doping of carbon materials have employed DDQ and F2-HCNQ. The former molecule possesses 16 π electrons with each CN cyano group contributing four π electrons and each C═C group and C═O group both contributing two further π electrons, respectively. For F2-HCNQ there is a total of 32 π electrons (four π electrons from each CN group and one from each sp^2 C atom), and we find that F2-HCNQ is a stronger reducing agent (and is a more thermally stable form) than the fluorine-substituted derivative of tetracyanoquinodimethane (TCNQ), F4-TCNQ. This stronger reducing behavior arises from the presence of the two extra cyano groups, which are stronger electron acceptors than the fluorine atoms (Hammett constants of 0.66 and 0.62, respectively). The electron affinity of F2-HCNQ was calculated to be 4.7 eV, similar to that of F4-TCNQ; however, the LUMO level of F2-HCNQ is particularly low lying at −6.55 eV, compared to −6.04 eV in the case of F4-TCNQ.

We find that both DDQ and F2-HCNQ molecules are strongly bound to graphene with a binding energy of 1.09 and 1.60 eV, respectively, with an acceptor behavior of 0.33 holes per DDQ molecule and 0.50 holes per F2-HCNQ molecule, respectively, transferred to graphene. The DOS of DDQ adsorbed on graphene (Figure 4a) has an acceptor peak 0.2 eV below E_D. Significant mixing of the bands occurs, as shown in Figure 4b, where a largely flat DDQ molecular impurity related level near the Fermi level bisects the graphene's π bands. The p-type doping by DDQ is seen to cause a 0.34 eV downward shift of the Fermi level, which is consistent with the strong charge transfer determined by the Hirshfeld charge partitioning calculations. Furthermore, the bond lengths of the functional groups in DDQ increase upon adsorption from 1.685 to 1.691 Å (C−Cl bonds), from 1.218 to 1.225 Å (C−O double bond), and from 1.164 to 1.165 Å (C−N triple bond), further confirmation of p-type doping. The Hirshfeld charge partitioning calculations show a partial charge of ∼0.06e on each of the CN groups and each of the C═O pairs, while the majority of the remaining transferred electron charge is distributed around the carbon ring and a relatively low partial

DOI: 10.1021/acsami.5b05140
ACS Appl. Mater. Interfaces 2015, 7, 22246−22255

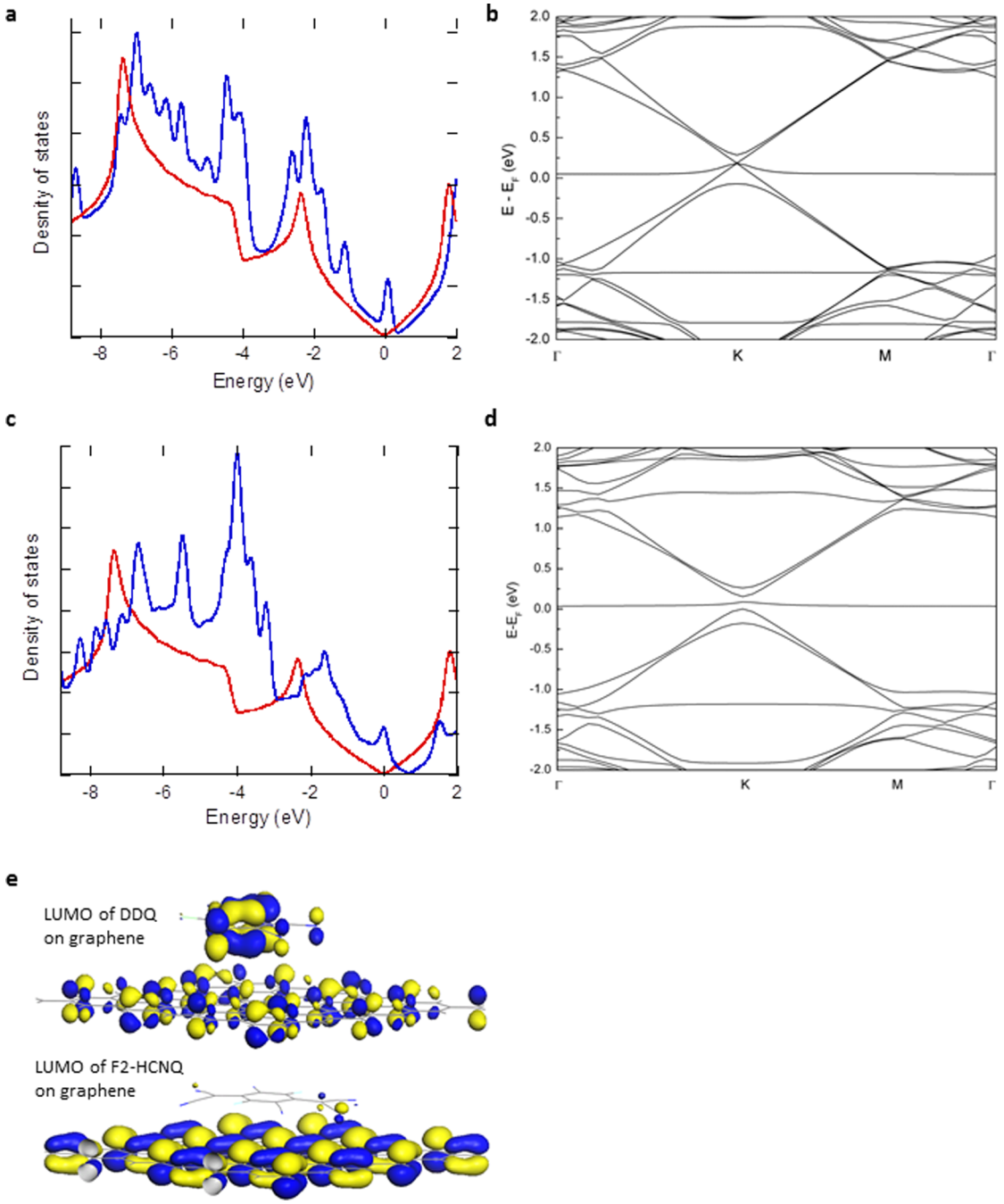

Figure 4. (a) Density of states of isolated graphene (red line) and DDQ adsorbed on graphene (blue line). (b) Band structure of DDQ adsorbed on graphene. (c) Density of states of isolated graphene (red line) and F2-HCNQ adsorbed on graphene (blue line). (d) Band structure of F2-HCNQ adsorbed on graphene. (e) LUMO of DDQ on graphene (upper figure) and of F2-HCNQ on graphene (lower figure) showing the effects of adsorption and delocalization.

charge of 0.02e is calculated for each of the Cl atoms. The stronger δ^- charges on the CN and O functional groups and the δ^+ charges on the underlying carbon atoms result in a tilted adsorption geometry due to the combination of electrostatic attraction and Pauli repulsion. This results in the nitrogen atoms of the CN groups and the oxygen atoms lying 0.2−0.3 Å closer to the graphene layer than the chlorine atoms. The energy levels of the HOMO and LUMO of DDQ are separated by ∼1.2 eV after the molecule has been adsorbed on the graphene layer, while the energies of the HOMO and LUMO levels for an isolated DDQ molecule are −7.85 and −6.19 eV, respectively, corresponding to a 1.66 eV energy separation. This change of HOMO−LUMO energy separation is nearly twice that found in the case of $CoCp_2$ adsorption, as reported earlier.

Density of states calculations arising from the adsorption of F2-HCNQ on graphene (Figure 4c) show a strong LUMO peak at 0.68 eV below E_D and significant mixing around the K point accompanied by the appearance of a band gap of 0.15 eV (Figure 4d). The partial charge on each of the outer CN functional groups is found to be approximately 0.06e, which causes an elongation of the outer CN group triple bond from 1.165 to 1.167 Å; the inner CN groups each have a partial charge of 0.03e and their bond lengths extend slightly from 1.163 to 1.164 Å, while the C−F bonds increase in length from

DOI: 10.1021/acsami.5b05140
ACS Appl. Mater. Interfaces 2015, 7, 22246−22255

1.314 to 1.322 Å. We further find that the carrier concentration in the F2-HCNQ-doped graphene is 53% higher than that in the F4-TCNQ-doped graphene, the next most effective p-type dopant. This confirms the superiority of F2-HCNQ as a particularly strong p-type dopant for graphene due to the additional two cyano groups that act as particularly strong electron acceptors. Significant changes to the shape of the LUMOs upon adsorption occur, as shown in Figure 4e, with near complete delocalization on graphene's π electron cloud upon adsorption of F2-HCNQ on graphene.

The appearance of an adsorbate-induced band gap (Figures 3c and 4d) may provide a way to a metal−insulator transition (MIT) if the Fermi level of previously unintentionally electron doped epitaxial SiC grown graphene can be moved into the band gap. Zhou et al.[33] showed a MIT using NO_2-doped epitaxial grown graphene; our calculations predict that the organic and organometallic molecules studied here may provide an attractive alternative approach, since the binding energy and charge transfers are larger than those found upon adsorption of NO_2. In addition, the need for patterning of the atoms or molecules is unnecessary to induce an energy gap, as in the case of hydrogen decoration.[34] More generally, organic and organometallic molecules can be used to modify the electronic properties of other materials that possess a similar low-lying-energy Dirac cone and a linear low-energy-dispersion behavior to graphene. Such materials include single-layer silicene[4,35] or three-dimensional topological insulator (TI) materials, where TI materials have time-reversal (TR) symmetry-protected gapless surface states. In the case of Bi_2Se_3, Bi_2Te_2, and Sb_2Te_3, these materials possess a Dirac cone on the surface where the spin-momentum locking can occur.[36] This Dirac cone is resilient to adsorbates that do not break TR symmetry; however, by choosing, for example, spin-polarized molecules such as cobaltocene, which can interact strongly, one can break TR symmetry. This provides another example of how molecular adsorption can be used as a route to modify the electronic properties of Dirac cone materials.

3.3. Electrical Characteristics. The significance of these charge transfer values, summarized in Table 1, can be related to electrical measurements and to frequency-dependent conductivity calculations. Many of the attractive electronic properties of graphene near E_D, where the π bonding and π^* antibonding states meet at the K points in the Brillouin zone, are as a result of graphene's linear band dispersion, $E(k) = \hbar v_F(k - K)$, where the Fermi velocity (v_F) is related to electron hopping between neighboring AB sublattices. From the corresponding low-energy linear DOS, the net carrier density is given by

$$n - p = \mathrm{sgn}(E_F)\frac{{E_F}^2}{\pi(\hbar v_F)^2} \tag{2}$$

where the Fermi energy (E_F, in eV) is measured relative to E_D. From eq 2, for a typical Fermi velocity of 10^6 m/s, the magnitude of the net carrier density (in units of cm^{-2}) is given approximately by $n - p = (7.4 \times 10^{13}){E_F}^2$.

A charge transfer of 0.24 electrons per molecule from TTF in a 6 × 6 supercell of area 18.9×10^{-15} cm^2, corresponding to a molecular surface coverage of 1.4%, results in an induced electron density of 1.3×10^{13} cm^{-2} and a Fermi level shift of 0.42 eV above E_D. For the case of DDQ adsorption, a charge transfer of 0.33 holes per molecule corresponds to an induced hole concentration of 1.8×10^{13} cm^{-2} and a Fermi level shift of 0.49 eV, a value more than sufficient to compensate for the unintentional Fermi level shift of 0.3 eV typically found during epitaxial growth on SiC wafers.[37] Finally, a charge transfer of 0.50 holes per F2-HCNQ molecule induces a hole concentration of 2.7×10^{13} cm^{-2} and Fermi level shift of 0.60 eV. Obtaining the same change in hole concentration in a typical electrical measurement (using 300 nm thick SiO_2 with a gate efficiency factor of 7.2×10^{10} cm^{-2} V^{-1}) requires changes in gate voltage of over 240 and 365 V, respectively. Such a voltage change would correspond to electric fields across the insulator that are in excess of the breakdown fields of SiO_2, thus demonstrating the importance of molecular doping as a way to functionalize graphene to adjust the carrier concentration.

The effect of doping on the high-frequency conductivity can be calculated, within the random-phase approximation,[12] by the equation below

$$\sigma(\omega) = \frac{2ie^2k_BT}{\pi\hbar^2(\omega + i/\tau)}\ln\left(2\cosh\left(\frac{E_F}{2k_BT}\right)\right) + \frac{e^2}{4\hbar}\left(\frac{1}{2} + \frac{1}{\pi}\tan^{-1}\left(\frac{\hbar\omega - 2E_F}{2k_BT}\right) - \frac{i}{2\pi}\ln\left(\frac{(\hbar\omega + 2E_F)^2}{(\hbar\omega - 2E_F)^2 + 4(k_BT)^2}\right)\right) \tag{3}$$

where k_B is Boltzmann's constant, T is temperature in kelvin, and τ is the carrier relaxation time. The first term in eq 3 is associated with intraband conduction (σ_{intra}) within a Drude-type formulism that has been modified to take account of nonzero temperature. The second term in eq 3 describes the contribution of interband conduction (σ_{inter}), which is responsible for the free carrier response and for which excitation between states with $\hbar\omega < 2|E_F|$ are Pauli-blocked. In the situation when $\hbar\omega \gg E_F, k_BT$, the real component of σ_{inter} tends to the limiting value of $\pi e^2/2h$. Figure 5 shows the variation of both the real and imaginary high-frequency conductivity, noting that the units of conductivity in two dimensions are S (not S/m as in 3D).

Two cases are considered: graphene n-doped with $CoCp_2$ to an electron concentration of 2.2×10^{13} cm^{-2}, corresponding to a Fermi energy of 0.54 eV (blue curves), and graphene doped with TTF to an electron concentration of 1.3×10^{13} cm^{-2}, corresponding to a Fermi energy of 0.42 eV (red curves). The temperature is taken as 300 K and the relaxation time is taken

Table 1. Summary of the Calculated Charge Transfer per Molecule in Units of Electron Charge with Positive (Negative) Values Corresponding to Hole (Electron) Doping of Graphene, the Number of π Electrons per Molecule, and Molecular Binding Energy per Adsorbed Molecule, Measured in eV

molecule	charge transfer per adsorbed molecule	number of π electrons per molecule	binding energy per adsorbed molecule (eV)
$FeCp_2$	+0.003e	12 in total, 6 per ring	0.42
$CoCp_2$	−0.41e	12 in total, 6 per ring	0.86
TTF	−0.24e	14	0.90−0.95
DDQ	+0.33e	16	1.09
F2-HCNQ	+0.50e	32	1.60

DOI: 10.1021/acsami.5b05140
ACS Appl. Mater. Interfaces 2015, 7, 22246−22255

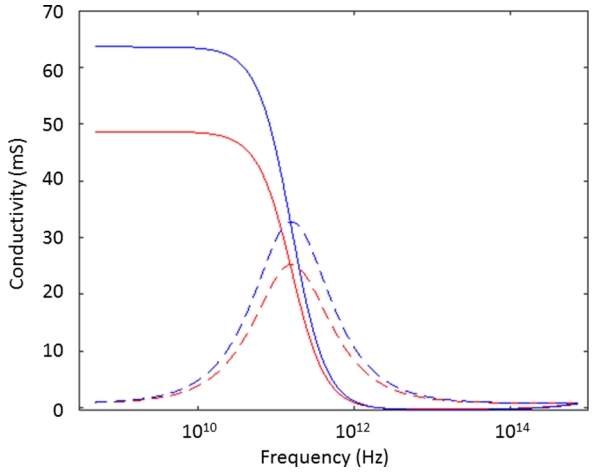

Figure 5. Variation of the real (solid line) and imaginary (dashed line) part of conductivity of doped graphene with 1.4% coverage of (i) $CoCp_2$ adsorbed on graphene corresponding to an electron concentration 2.2×10^{13} cm^{-2} (blue curves) and (ii) TTF adsorbed on graphene, corresponding to an electron concentration 1.3×10^{13} cm^{-2} (red curves). A carrier relaxation time of 1 ps and a temperature of 300 K is used via eq 3.

as 1 ps.[2] The real part of the conductivity is found to exhibit a largely dispersion-less behavior in the dc−gigahertz regime at about 49 and 64 mS, respectively, for the two doping levels, without a significant contribution from the imaginary component of conductivity in this frequency range. These values of the real part of σ, in units of mS, are consistent with the dc conductivity calculated from

$$\sigma(0) = \frac{e^2 E_F \tau}{\pi \hbar^2} = 118 E_F \tau \quad (4)$$

with the value of E_F measured in electronvolts above the Dirac point and τ measured in picoseconds. The cutoff frequency of a graphene transistor is approximately proportional to the transconductance and inversely proportional to the source/drain capacitance and resistance. Increasing the conductivity leads to higher drain current and hence larger transconductance, depending on the capacitive coupling from the gate. In the study by Lin et al.,[38] they reported a measured transconductance of 45 mS per mm of device width, which for a device of about 40 μm in width corresponds to a measured transconductance of about 1.6 mS. Our value of conductivity, 65 mS, is thus very encouraging for high-frequency applications, as the conductivity can be scaled by suitable choice of device width and channel length to give the desired high device conductance for operation.

In addition to the magnitude of the conductivity, discussion of dispersion behavior with other conductors and antenna materials is useful at this point. In the gigahertz frequency range the electrical losses of metals usually increase with increasing frequency. This behavior has been experimentally verified through measurements made on millimeter-long coplanar waveguides (CPWs) fabricated from both microsized silver and nanosized silver grains and showed that the microwave insertion losses are around 0.4 dB/mm at 20 GHz, which steadily increased at a rate of 0.1 dB/mm per GHz frequency change.[39] This is a result of the conduction being constrained to a thin surface layer due to the skin effect and the greater contribution of surface roughness losses. For graphene, such surface roughness losses are not expected to be significant. A similar dispersion-less behavior in the frequency range between 40 and 110 GHz has been previously reported in CPWs fabricated from multiwalled carbon nanotube−polymer composites with losses as low as 0.15 dB/mm and attributed to the capacitive coupling between the nanotubes surrounded by a thin polymer coating.[40] In this case, the polymer coating acts as a tunnel barrier for electrons, provided that the nanotube volume fraction exceeds the percolation threshold. Skulason et al. report that microwave measurements made on CVD-grown graphene CPW structures also reveal a negligible dependence on frequency up to 110 GHz.[41] They attribute this behavior to an insignificant influence of the skin effect and negligible kinetic inductance. For practical applications at microwave frequencies, the presence of largely frequency independent conductivity behavior is potentially important for broadband applications, such as half-wavelength filter, quarter-wavelength coupler, fast switches and modulators, millimeter-wave links for high data rate transfer.

At terahertz frequencies, the intraband transitions yield localized graphene plasmons, which in graphene are highly confined. Control of the plasmon frequency is easier in graphene than with metals, as the carrier concentration can be more readily tuned in graphene than in metals. The real and imaginary parts of the conductivity can be related to the frequency-dependent dielectric and to the refractive index. As a result, the presence of dopant molecules acts to locally adjust the carrier concentration and the refractive index in the form of a localized molecular gating effect. At higher frequencies, when the Fermi level is away from the Dirac point, then only photons with $\hbar\omega > 2|E_F|$ are absorbed and contribute to the conductivity; this is a key feature of a graphene-based electroabsorptive modulator, where experimental modulation of 0.1 dB/μm from 1.35 to 1.6 μm, corresponding to $(2.2-1.87) \times 10^{14}$ Hz, has been reported.[42] Potential applications which can make use of the lightweight and flexible nature of graphene and which operate at the frequency bands discussed here include conformal and reconfigurable antennas for high rates of data transfer, personalized and wearable mobile communications, and wireless and body sensor networks, where the biocompatible properties of graphene could be a significant advantage. In addition, the development of giga- and terahertz sources and detection may play a role in the development of compact imaging for health diagnostics and security screening.

4. SUMMARY

In conclusion, our ab initio DFT calculations have allowed us to demonstrate the potential of molecular doping to achieve high charge transfer efficiencies, leading to high carrier densities and high-frequency conductivity in single-layer graphene. Efficient n-type doping is found using cobaltocene without introducing detrimental effects to the graphene band structure, which would lower mobility. High levels of doping, both n- or p-type, are found with the organic molecules TTF, DDQ, and F2-HCNQ, though the stronger $\pi-\pi$ interaction also results in significant mixing between the molecule and graphene's π electron states, which disrupts the linearity of the bands. The high frequency electrical conductivity has been calculated and is found to be to be largely frequency-independent over a wide range of gigahertz frequencies and shows high conductivity up to 65 mS in n-doped material, suitable for a wide range of high-frequency applications.

DOI: 10.1021/acsami.5b05140
ACS Appl. Mater. Interfaces 2015, 7, 22246−22255

AUTHOR INFORMATION

Corresponding Author

*E-mail: David.Carey@surrey.ac.uk.

Notes

The authors declare no competing financial interest.

ACKNOWLEDGMENTS

A.J.S. acknowledges prior research student support from the Engineering and Physical Sciences Research Council (EPSRC, UK). J.D.C. acknowledges current support for graphene research from EPSRC Grant EP/L02263X/1. The authors confirm that data underlying the findings are available without restriction. Details on the data and how to request access are available from the University of Surrey Publications Repository.

REFERENCES

(1) Geim, A.; Grigorieva, I. van der Waals Heterostructures. *Nature* **2013**, *499*, 419−425.

(2) Novoselov, K.; Geim, A. K.; Morozov, S. V.; Jiang, D.; Zhang, Y.; Dubonas, S. V.; Grigorieva, I. V.; Firsov, A. A. Electric Field Effect in Atomically Thin Carbon Films. *Science* **2004**, *306*, 666−669.

(3) Li, L.; Yu, Y.; Ye, G. J.; Ge, Q.; Ou, X.; Wu, H.; Feng, D.; Chen, X. H.; Zhang, Y. Black Phosphorus Field-Effect Transistors. *Nat. Nanotechnol.* **2014**, *9*, 372−377.

(4) Tao, L.; Cinquanta, E.; Chiappe, D.; Grazianetti, C.; Fanciulli, M.; Dubey, M.; Molle, A.; Akinwande, D. Silicene Field-Effect Transistors Operating at Room Temperature. *Nat. Nanotechnol.* **2015**, *10*, 227−231.

(5) Wang, Q.; Kalantar-Zadeh, K.; Kis, A.; Coleman, J.; Strano, M. Electronics and Optoelectronics of Two-Dimensional Transition Metal Dichalcogenides. *Nat. Nanotechnol.* **2012**, *7*, 699−712.

(6) Sun, Z.; Liao, T.; Dou, Y.; Hwang, S.; Park, M.; Jiang, L.; Kim, J.; Dou, S. Generalized Self-Assembly of Scalable Two-Dimensional Transition Metal Oxide Nanosheets. *Nat. Commun.* **2014**, *5*, 3813.

(7) Zhang, Y.; Tan, Y.; Stormer, H.; Kim, P. Experimental Observation of the Quantum Hall Effect and Berry's Phase in Graphene. *Nature* **2005**, *438*, 201−204.

(8) Tzalenchuk, A.; Lara-Avila, S.; Kalaboukhov, A.; Paolillo, S.; Syväjärvi, M.; Yakimova, R.; Kazakova, O.; Janssen, T.; Fal'ko, V.; Kubatkin, S. Towards a Quantum Resistance Standard Based on Epitaxial Graphene. *Nat. Nanotechnol.* **2010**, *5*, 186−189.

(9) Wang, X.; Zhi, L.; Müllen, K. Transparent, Conductive Graphene Electrodes for Dye-Sensitized Solar Cells. *Nano Lett.* **2008**, *8*, 323−327.

(10) Lin, Y.; Dimitrakopoulos, C.; Jenkins, K.; Farmer, D.; Chiu, H.; Grill, A.; Avouris, P. 100-GHz Transistors from Wafer-Scale Epitaxial Graphene. *Science* **2010**, *327*, 662−662.

(11) Low, T.; Avouris, P. Graphene Plasmonics for Terahertz to Mid-Infrared Applications. *ACS Nano* **2014**, *8*, 1086−1101.

(12) Yao, Y.; Kats, M.; Genevet, P.; Yu, N.; Song, Y.; Kong, J.; Capasso, F. Broad Electrical Tuning of Graphene-Loaded Plasmonic Antennas. *Nano Lett.* **2013**, *13*, 1257−1264.

(13) Novoselov, K.; Fal'ko, V.; Colombo, L.; Gellert, P.; Schwab, M.; Kim, K. A Roadmap for Graphene. *Nature* **2012**, *490*, 192−200.

(14) Ahn, J.; Hong, B. Graphene for Displays that Bend. *Nat. Nanotechnol.* **2014**, *9*, 737−738.

(15) Schall, D.; Neumaier, D.; Mohsin, M.; Chmielak, B.; Bolten, J.; Porschatis, C.; Prinzen, A.; Matheisen, C.; Kuebart, W.; Junginger, B.; Templ, W.; Giesecke, A. L.; Kurz, H. 50 GBit/s Photodetectors Based on Wafer-Scale Graphene for Integrated Silicon Photonic Communication Systems. *ACS Photonics* **2014**, *1*, 781−784.

(16) Bonaccorso, F.; Sun, Z.; Hasan, T.; Ferrari, A. C. Graphene Photonics and Optoelectronics. *Nat. Photonics* **2010**, *4*, 611−622.

(17) Baeumer, C.; Saldana-Greco, D.; Martirez, J.; Rappe, A.; Shim, M.; Martin, L. Ferroelectrically Driven Spatial Carrier Density Modulation in Graphene. *Nat. Commun.* **2015**, *6*, 6136.

(18) Zhao, L.; He, R.; Rim, K.; Schiros, T.; Kim, K.; Zhou, H.; Gutierrez, C.; Chockalingam, S.; Arguello, C.; Palova, L.; Nordlund, D.; Hybertsen, M.; Reichman, D.; Heinz, T.; Kim, P.; Pinczuk, A.; Flynn, G.; Pasupathy, A. Visualizing Individual Nitrogen Dopants in Monolayer Graphene. *Science* **2011**, *333*, 999−1003.

(19) Marchenko, D.; Varykhalov, A.; Scholz, M.; Bihlmayer, G.; Rashba, E.; Rybkin, A.; Shikin, A.; Rader, O. Giant Rashba Splitting in Graphene Due to Hybridization with Gold. *Nat. Commun.* **2012**, *3*, 1232.

(20) Pi, K.; Han, W.; McCreary, K.; Swartz, A.; Li, Y.; Kawakami, R. Manipulation of Spin Transport in Graphene by Surface Chemical Doping. *Phys. Rev. Lett.* **2010**, *104*, 187201.

(21) Cheng, J.; Wang, W.; Mosallaei, H.; Kaxiras, E. Surface Plasmon Engineering in Graphene Functionalized with Organic Molecules: A Multiscale Theoretical Investigation. *Nano Lett.* **2014**, *14*, 50−56.

(22) Leenaerts, O.; Partoens, B.; Peeters, F. Adsorption of H_2O, NH_3, CO, NO_2, and NO on Graphene: A First-Principles Study. *Phys. Rev. B* **2008**, *77*, 125416.

(23) Romero, H.; Joshi, P.; Gupta, A.; Gutierrez, H.; Cole, M.; Tadigadapa, S.; Eklund, P. Adsorption of Ammonia on Graphene. *Nanotechnology* **2009**, *20*, 245501.

(24) Lee, B.; Chen, Y.; Duerr, F.; Mastrogiovanni, D.; Garfunkel, E.; Andrei, E.; Podzorov, V. Modification of Electronic Properties of Graphene with Self-Assembled Monolayers. *Nano Lett.* **2010**, *10*, 2427−2432.

(25) Bae, S.; Kahya, O.; Sharma, B.; Kwon, J.; Cho, H.; Özyilmaz, B.; Ahn, J. Graphene-P(VDF-TrFE) Multilayer Film for Flexible Applications. *ACS Nano* **2013**, *7*, 3130−3138.

(26) Ni, G.; Zheng, Y.; Bae, S.; Tan, C.; Kahya, O.; Wu, J.; Hong, B.; Yao, K.; Özyilmaz, B. Graphene−Ferroelectric Hybrid Structure for Flexible Transparent Electrodes. *ACS Nano* **2012**, *6*, 3935−3942.

(27) Alves, H.; Molinari, A.; Xie, H.; Morpurgo, A. Metallic Conduction at Organic Charge-Transfer Interfaces. *Nat. Mater.* **2008**, *7*, 574−580.

(28) Vosko, S.; Wilk, L.; Nusair, M. Accurate Spin-Dependent Electron Liquid Correlation Energies For Local Spin Density Calculations: A Critical Analysis. *Can. J. Phys.* **1980**, *58*, 1200−1211.

(29) Henwood, D.; Carey, J. D. *Ab initio* Investigation of Molecular Hydrogen Physisorption on Graphene and Carbon Nanotubes. *Phys. Rev. B* **2007**, *75*, 245413.

(30) Wehling, T.; Yuan, S.; Lichtenstein, A.; Geim, A.; Katsnelson, M. Resonant Scattering by Realistic Impurities in Graphene. *Phys. Rev. Lett.* **2010**, *105*, 056802.

(31) Takenobu, T.; Takano, T.; Shiraishi, M.; Murakami, Y.; Ata, M.; Kataura, H.; Achiba, Y.; Iwasa, Y. Stable and Controlled Amphoteric Doping by Encapsulation of Organic Molecules Inside Carbon Nanotubes. *Nat. Mater.* **2003**, *2*, 683−688.

(32) Samuels, A.; Carey, J. D. Molecular Doping and Band-Gap Opening of Bilayer Graphene. *ACS Nano* **2013**, *7*, 2790−2799.

(33) Zhou, S.; Siegel, D.; Fedorov, A.; Lanzara, A. Metal to Insulator Transition in Epitaxial Graphene Induced by Molecular Doping. *Phys. Rev. Lett.* **2008**, *101*, 086402.

(34) Balog, R.; Jørgensen, B.; Nilsson, L.; Andersen, M.; Rienks, E.; Bianchi, M.; Fanetti, M.; Lægsgaard, E.; Baraldi, A.; Lizzit, S.; Sljivancanin, Z.; Besenbacher, F.; Hammer, B.; Pedersen, T.; Hofmann, P.; Hornekær, L. Bandgap Opening in Graphene Induced by Patterned Hydrogen Adsorption. *Nat. Mater.* **2010**, *9*, 315−319.

(35) Roome, N. J.; Carey, J. D. Beyond Graphene: Stable Elemental Monolayers of Silicene and Germanene. *ACS Appl. Mater. Interfaces* **2014**, *6*, 7743−7750.

(36) Zhang, H.; Liu, C.; Qi, X.; Dai, X.; Fang, Z.; Zhang, S. Topological Insulators in Bi_2Se_3, Bi_2Te_3 and Sb_2Te_3 with a Single Dirac Cone on the Surface. *Nat. Phys.* **2009**, *5*, 438−442.

(37) Coletti, C.; Riedl, C.; Lee, D.; Krauss, B.; Patthey, L.; von Klitzing, K.; Smet, J.; Starke, U. Charge Neutrality and Band-Gap Tuning of Epitaxial Graphene on SiC by Molecular Doping. *Phys. Rev. B* **2010**, *81*, 235401.

DOI: 10.1021/acsami.5b05140
ACS Appl. Mater. Interfaces 2015, 7, 22246−22255

(38) Lin, Y.; Jenkins, K.; Valdes-Garcia, A.; Small, J.; Farmer, D.; Avouris, P. Operation of Graphene Transistors at Gigahertz Frequencies. *Nano Lett.* **2009**, *9*, 422−426.
(39) Alshehri, A.; Jakubowska, M.; Młożniak, A.; Horaczek, M.; Rudka, D.; Free, C.; Carey, J. D. Enhanced Electrical Conductivity of Silver Nanoparticles for High Frequency Electronic Applications. *ACS Appl. Mater. Interfaces* **2012**, *4*, 7007−7010.
(40) Alshehri, A.; Jakubowska, M.; Sloma, M.; Horaczek, M.; Rudka, D.; Free, C.; Carey, J. D. Electrical Performance of Carbon Nanotube-Polymer Composites at Frequencies up to 220 GHz. *Appl. Phys. Lett.* **2011**, *99*, 153109.
(41) Skulason, H.; Nguyen, H.; Guermoune, A.; Sridharan, V.; Siaj, M.; Caloz, C.; Szkopek, T. 110 GHz measurement of large-area graphene integrated in low-loss microwave structures. *Appl. Phys. Lett.* **2011**, *99*, 153504.
(42) Liu, M.; Yin, X.; Ulin-Avila, E.; Geng, B.; Zentgraf, T.; Ju, L.; Wang, F.; Zhang, X. A Graphene-Based Broadband Optical Modulator. *Nature* **2011**, *474*, 64−67.

DOI: 10.1021/acsami.5b05140
ACS Appl. Mater. Interfaces 2015, 7, 22246−22255